Vol. 08, No. 1 (2026) 1-12, doi: 10.24874/PES08.01.001

Proceedings on Engineering Sciences

www.pesjournal.net

NUMERICAL SIMULATION OF VORTEX-INDUCED VIBRATIONS OF TWO TANDEM CIRCULAR STRUCTURES IN OSCILLATORY FLOW

Henry Francis Annapeh
Victoria Kurushina[1]

Received 13.03.2025.
Revised 26.06.2025.
Accepted 17.07.2025.

Keywords:

Vortex-induced vibration, VIV, Oscillatory flow, Tandem cylinders, Two degree-of-freedom structure

A B S T R A C T

This study investigates vortex-induced vibration (VIV) of two tandem circular cylinders with two degrees of freedom (2DOF) under a pure oscillatory flow. Numerical simulations are performed using a detached eddy simulation solver with the k-ω SST turbulence model, and the results are validated against existing data. The maximum transverse amplitude occurs at a reduced velocity of 10, coinciding with the lock-in regime, while the single isolated cylinder shows a higher amplitude than the tandem setup. Streamwise displacement amplitude exceeds 2.5D for the considered cases. Frequency analysis reveals mode transitions from double to single-frequency modes as the reduced velocity increases. XY trajectory patterns vary with velocity, showing infinity (∞), arc-like, O-shape, and net-like forms. This study enhances understanding of VIV in tandem cylinders and provides insights for engineering applications.

1. INTRODUCTION

These are instructions for authors and this document has Ocean environments pose a number of challenges for the design of subsea slender structures. One such challenge is the prediction of vortex-induced vibrations (VIV), which must be carefully considered in the design of risers and subsea cables. VIV arises when structural vibrations are triggered by vortex formation around a bluff body. VIV effects become particularly significant when the frequency of vortex shedding approaches the natural frequency of the structure, leading to the "lock-in" condition, characterized by increased displacement amplitudes. This type of vibration can significantly accelerate fatigue damage accumulation over the structure's lifespan, potentially resulting in downtime and failure. The phenomenon is sensitive to a broad range of structural and flow parameters, and oscillatory flows, linked to variations in velocity and direction, introduce additional complexity, including complications to the potential lock-in state.

A fundamental mapping of the vortex shedding regimes in terms of the Keulegan-Carpenter (*KC*) number (Keulegan and Carpenter, 1958), ranging from 2 to 40, is presented in Williamson (1985). In this experimental work (Williamson, 1985), the *KC* number from 2 to 4 is identified as (1) a symmetric non-shedding regime; *KC* number from 4 to 7 as (2) an asymmetric non-shedding regime; *KC* number from 7 to 15 as (3) a single-pair

[1] Corresponding author: Victoria Kurushina
Email: v.kurushina@outlook.com

regime; *KC* number from 15 to 24 as (4) a double-pair regime; *KC* number from 24 to 32 as (5) a three-pair regime; and *KC* number from 32 to 40 as (6) a four-pair regime. These regime boundaries have also been investigated in Bearman et al. (1985), Tatsuno and Bearman (1990), Justesen (1991), and are known to be influenced by the Reynolds number (Re) (Sumer and Fredsøe, 1997). Together with studies by Bearman (1984), Sarpkaya and Storm (1985), Sarpkaya (1986), Obasaju et al. (1988), Meneghini and Bearman (1995), these works have laid a strong foundation for a wide range of modern research on oscillatory flow.

Oscillatory flow is closely linked to the phenomenon of steady streaming, which is discussed in detail in An et al. (2009). Steady streaming refers to a non-zero period-averaged flow field around a cylinder in oscillatory flow, even when the mean velocity of the external flow is zero. The numerical study by An et al. (2009) investigates this effect for *KC* numbers of 3.5, 5, 10, 16, 26 and 33, with a Stokes number of 196, which is another key dimensionless number characterizing oscillatory flows. This work finds six steady streaming patterns, corresponding to the six oscillatory flow regimes, and also classifies the known regimes into two groups. The first identified group, comprising the flow regimes (1,2,3,5), is characterized by half-period symmetric flow structure and symmetric steady streaming. The second group, including regimes (4,6), is associated with anti-symmetric oscillatory flow structures and anti-symmetric steady streaming. Related studies have also explored hydrodynamics forces acting on a structure in oscillatory flow (An, 2009), as well as the behavior at low *KC* numbers (An et al., 2011).

Another pattern observed in oscillatory flows is the time-varying behavior of drag and added mass coefficients, which is particularly relevant to flexible structures, as discussed in Ren et al. (2020) for the *KC* numbers ranging from 10 to 178. This experimental study considers a reduced velocity (U_r) range from 4 to 7.9 and compares the results between vibrating and stationary structures. This research reveals high-frequency components and hysteresis in the hydrodynamic force acting on the structure and highlights differences between the hysteresis observed in the VIV response and in the force: the hydrodynamics force is higher during the acceleration phase of the flow oscillation cycle, whereas the opposite trend is reported in the literature for structural vibrations. Additionally, the maximum drag coefficient of a vibrating structure reaches 3.5 for $KC < 30$, indicating substantial amplification at low *KC* numbers. This investigation also proposes an empirical mean drag coefficient prediction formula based on the obtained experimental results; however, reveals no clear pattern in changes of added mass coefficients with reduced velocity. This line of research is continued in Zhang et al. (2022) with the proposition of the dimensionless acceleration parameter.

VIV in oscillatory flows is also strongly associated with variations in structural response during the lock-in state, as observed experimentally in Barbi et al. (1986). In Zhao et al. (2012), oscillatory flow is investigated numerically for the *KC* numbers of 10 and 20, with the reduced velocities ranging from 1 to 36. The study identifies a single-frequency vibration mode for both the *KC* numbers at $U_r < 8$. The research reveals the differences in the lock-in region in terms of the vibration amplitude and mean displacement value between the two *KC* cases. The research Zhao et al. (2013) numerically explores VIV in a combined steady and oscillatory flow at a *KC* number of 10, with reduced velocities, ranging from 2 to 25. The study reveals that cross-flow vibrations lock onto twice the oscillatory flow frequency, when the flow ratio α is ≤ 0.2, and onto the natural frequency of the structure when $\alpha \geq 0.6$. The investigation finds that the lock-in region is broader in the reduced velocity range than in either steady or purely oscillatory flow alone. Also, three different vortex shedding modes are observed during a single period of oscillatory flow at $\alpha = 0.8$ and $Ur = 7$.
A numerical study for a two-degree-of-freedom (2DOF) rigid structure VIV is presented in Zhao (2013) for *KC* numbers of 10, 20 and 40. The investigation reveals multiple frequency peaks in the structural response for $KC = 20$ and 40. The observed response of structure is classified as single-frequency, double-frequency and triple-frequency modes. The paper discusses the transition between in-phase and anti-phase vibration regimes in the cross-flow direction, identifying reduced velocity thresholds of 7, 9, and 11 for *KC* of 10, 20, and 40, respectively. Both regular and irregular vibration patterns are reported. For in-line motion, the dominant vibration frequency corresponds to the oscillatory flow frequency, and its amplitude exceeds that of other frequency components. Moreover, the peak frequencies observed in the cross-flow direction are also present in the in-line response.

A specialized branch of oscillatory flow studies focuses on multiple bluff bodies, likely originating from laboratory tests involving single structure, two cylinders and 3 x 3 array, as reported in Bushnell (1977, May). Numerical and experimental investigations of two tandem and one staggered cylinder configurations in subcritical oscillatory flow are presented in Skomedal et al. (1989). A later study by An et al. (2006) performs numerical simulations for two circular cylinders with small, moderate and large gaps for $KC = 10$, 20, and 28. This investigation reveals the formation of complex, oblique, and independent vortex streets behind the structures, corresponding to the three distinct gap ratios. The findings also demonstrate a pattern in the root-mean-square (RMS) in-line force coefficients: the coefficient on the upstream cylinder increases relative to the downstream cylinder as the gap ratio decreases.

Two square cylinders in a side-by-side configuration in oscillatory flow are examined in Chern et al. (2010) for *KC* numbers ranging from 1 to 15 and gap ratios from 0.5

to 2.0. The formation of symmetric vortices around the square structures is reported up to *KC* = 7, followed by a transitional region, and the onset of asymmetric vortex shedding starting at *KC* = 10 and above. The study also proposes an empirical correlation between the *KC* number and the in-line force coefficient for various gap ratios.

Tandem and side-by-side arrangements of circular cylinders in oscillatory flow are further investigated numerically in Zhao and Cheng (2014). Simulations are performed for gap ratios from 0.5 to 4.0 and *KC* numbers ranging from 1 to 12. For the side-by-side configuration, gap vortex shedding and combined flow regimes are identified at smaller gap ratios.

Recent research on circular cylinders by Lu et al. (2023) reports results for tandem, staggered, and side-by-side configurations by varying the flow incidence angle from 0^o to 90^o. The study focuses on gap ratios from 0.5 to 4.0 and *KC* numbers from 4 to 12. This investigation reveals four flow regimes for the tandem and side-by-side cases, and eleven distinct flow regimes for staggered cylinders, depending on the incidence angle.

Structures of different diameters in oscillatory flow are explored in An et al. (2006, January), Pearcey et al. (2017). In Pearcey et al. (2017), one of the cylinders is significantly smaller than the main elastically mounted structure, while cylinders are rigidly connected. The study considers *KC* = 10, varying the flow incidence angle and gap ratio. This research discovers several vortex shedding regimes, some appearing at $U_r > 10$. The study also reports a single-vortex regime, in which a vortex effectively rotates around the larger structure. In this regime, the lift force frequency synchronizes with the oscillatory flow frequency.

Oscillatory flow over four structures is thoroughly investigated for a square layout in Tong et al. (2015) and a diamond layout in Ren et al. (2019). The study in Tong et al. (2015) presents a numerical analysis of gap ratio effects for *KC* numbers ranging from 1 to 12, enabling the observation of transitions from a single-body vortex shedding mode to distinct individual flow structures. The study identifies several reflection symmetry regimes, spatio-temporal symmetry regimes and symmetry-breaking flow patterns. The diamond arrangement is investigated in Ren et al. (2019) for *KC* numbers ranging from 4 to 12 and gap ratios from 0.5 to 4.0, revealing synchronous, quasi-periodic and desynchronized flow types within the parameter space. The study reports the flow maps in terms of the *KC* and *Re* numbers for each gap ratio, expanding findings of Tatsuno and Bearman (1990) and Pearcey et al. (2017), and revealing physical mechanisms behind map holes.

Despite significant progress in mapping the vortex shedding regimes and identifying patterns in hydrodynamic forcing, there remains a lack of literature on changes to lock-in peaks in oscillatory flows involving rigid structures with two degrees of freedom arranged in an array layout. Majority of the reviewed studies consider cross-flow vibration only or stationary structures. Based on the literature analysis, the current study aims to investigate two circular cylinders in tandem within a sinusoidal oscillatory flow at *KC* = 10.

2. MODEL

2.1 Computational model

This study focuses on simulating vortex-induced vibrations (VIV) of two tandem circular cylinders with two degrees of freedom (2DOF) subjected to sinusoidal oscillatory flow. The computational domain, shown in Figure 1, measures 60*D* × 40*D*, where *D* is the diameter of the cylinders (0.02 m). The upstream cylinder is positioned 20D from the inlet boundary to minimize inlet effects.

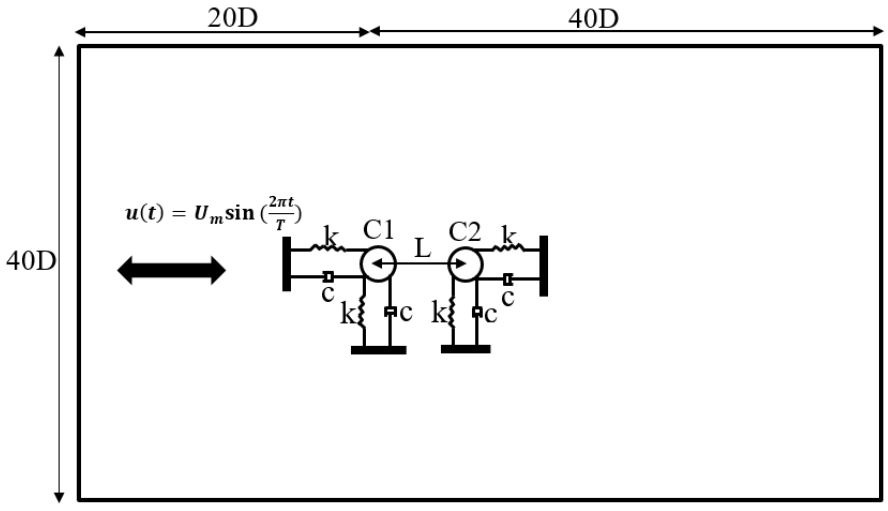

Figure 1. Computational domain for the simulation

The center-to-center spacing between the two cylinders is varied between 0.05 m and 0.09 m, corresponding to spacing ratios of 2.5, 3.5, and 4.5.
Boundary conditions include:

- Inlet (Left Boundary): velocity-inlet.
- Outlet (Right Boundary): pressure-outlet with zero-gauge pressure.
- Top and Bottom Boundaries: symmetry conditions.
- Cylinder Surfaces: no-slip wall condition.

A mass ratio of 1.62 is chosen to reflect typical submerged structural behavior in water, which is often defined by low mass ratios. The range of the Reynolds number of 615–6154 is selected to capture a fully turbulent flow regime. A range of reduced velocity from 2-20 is chosen to cover conditions where lock-in occurs for rigid structures ensuring the observation of initial, supper-upper and lower branch of the lock-in peak. This range of reduced velocity also enables the analysis of multiple dynamic regimes including the start of vortex shedding, maximum vibration amplitude and post-lock-in response.

2.2 Flow model

The oscillatory inflow velocity at the domain inlet is defined as:

$$u(t) = U_m \sin\left(\frac{2\pi t}{T}\right), \quad (1)$$

where U_m is the velocity amplitude, T is the oscillation period, and t is the time.

The governing dimensionless parameters include the Reynolds number:

$$Re = \frac{\rho U_m D}{\mu}, \quad (2)$$

and Keulegan-Carpenter number (KC):

$$KC = \frac{U_m T}{D}. \quad (3)$$

This study assumes KC = 10 throughout the simulations.

A Detached Eddy Simulation (DES) approach is used for turbulence modeling, combining the strengths of Reynolds-Averaged Navier-Stokes (RANS) for near-wall treatment and Large Eddy Simulation (LES) for capturing large-scale turbulent structures. The k–ω SST turbulence model is adopted alongside the PISO pressure-velocity coupling scheme. Time integration is conducted with a time step of 0.005 s.

The DES method incorporates both Reynolds-Averaged Navier-Stokes (RANS) and Large Eddy Simulation (LES) approaches, as in Annapeh and Kurushina (2024). The continuity and momentum equation of RANS for incompressible flow are given as follows:

$$\frac{\partial(\rho\overline{u_i})}{\partial x_i} = 0, \quad (4)$$

$$\frac{\partial(\rho\overline{u_i})}{\partial t} + \frac{\partial}{\partial x_j}\left(\rho\overline{u_i u_j} + \rho\overline{u_i' u_j'}\right) = \frac{\partial \bar{p}}{\partial x_i} + \frac{\partial \overline{\tau_{ij}}}{\partial x_j}, \quad (5)$$

where p is the mean pressure, $\overline{u_i}$ means the average Cartesian components of the velocity vector, $\rho\overline{u_i' u_j'}$ are the Reynolds stresses, ρ is the density of the fluid and $\overline{\tau_{ij}}$ is the mean viscous stress vector components, as follows:

$$\overline{\tau_{ij}} = \mu\left(\frac{\partial \overline{u_i}}{\partial x_j} + \frac{\partial \overline{u_j}}{\partial x_i}\right), \quad (6)$$

where μ denotes the dynamic viscosity. The Large Eddy Simulation (LES) method is based on the spatially filtered Navier-Stokes equation, and for the incompressible flow this system is as follows:

$$\frac{\partial \overline{u_i}}{\partial x_i} = 0, \quad (7)$$

$$\frac{\partial(\overline{u_i})}{\partial t} + \frac{\partial}{\partial x_j}\left(u_i u_j\right) = -\frac{1}{\rho}\frac{\partial \bar{p}}{\partial x_i} + \nu\frac{\partial^2 \overline{u_i}}{\partial x_j \partial x_j} - \frac{\partial \overline{\tau_{ij}}}{\partial x_j}, \quad (8)$$

where $\overline{u_i}$ and $\bar{p}$ represent the resolved filtered velocity and pressure, respectively.

The diffusion term of the DES model is as follows:

$$Y_k = \rho\beta^* k\omega F_{DES}, \quad (9)$$

where β^* is the constant of the SST model, k denotes fluctuation of the turbulent kinetic energy, ω is the specific energy dissipation rate, and F_{DES} is expressed as:

$$F_{DES} = \max\left(\frac{L_t}{C_{des}\Delta_{max}}, 1\right), \quad (10)$$

where C_{des} is a calibration constant used in the DES model with a value of 0.61, Δ_{max} is the local maximum grid map $\Delta = (\Delta_1, \Delta_2, \Delta_3)^{\frac{1}{3}}$. The turbulent length scale L_t is:

$$L_t = \frac{\sqrt{k}}{\beta^*\omega}. \quad (11)$$

2.3 Structural model

Each cylinder is modeled as an elastically mounted spring-mass-damper system with two degrees of freedom motion. The in-line displacement X and cross-flow displacement Y of a cylinder are given by the equations:

$$m_s\ddot{X} + r_s\dot{X} + kX = F_X, \quad (12)$$

$$m_s\ddot{Y} + r_s\dot{Y} + kY = F_Y, \quad (13)$$

where m_s is Structural mass, $r_s = 2\zeta\omega_n m_e$ is the damping coefficient, ζ is damping ratio, ω_n is natural frequency of the cylinder, m_e is effective mass, and k is stiffness coefficient.

Table 1 shows physical parameters used for the simulation.

Table 1. Physical parameters

Parameters	Values
Diameter, D [m]	0.02
Mass ratio, m^*	1.62
Natural frequency, f_n [Hz]	0.77
Reduced velocity, U_r	2-20
Reynolds number, *Re*	615-4615
Damping ratio, ζ	0.012
Keulegan-Carpenter number, *KC*	10

The mass ratio m^* of the moving cylinder is defined as:

$$m^* = \frac{m}{m_{fd}}, \tag{14}$$

where m_{fd} represents the displaced fluid mass, or:

$$m_{fd} = \frac{\rho_f D^2 \pi}{4}. \tag{15}$$

The reduced velocity U_r is defined as:

$$U_r = \frac{U_m}{f_n D}, \tag{16}$$

where f_n is given by:

$$f_n = \frac{1}{2\pi}\sqrt{\frac{k}{m_e}}, \tag{17}$$

where

$$m_e = \frac{\rho_f D^2 \pi C_A}{4} + m_s, \tag{18}$$

where $C_A = 1$ is the fluid added mass coefficient.

2.4 Mesh independence test and model validation

A mesh independence study is carried out using a single 2DOF circular cylinder under uniform flow to validate the grid design. Four mesh configurations are tested using the setup described in Tu et al. (2015), He et al. (2012) and Prasanth and Mittal (2008), with damping ratio ζ = 0 and time step 0.005 s. Near-cylinder regions are refined with a minimum element size of 0.00025 m. The results for the mesh independence test are presented in Table 2, along with details of the mesh configurations. The results are compared with published studies and show excellent agreement. The selected grid resolution is illustrated in Figure 2.

Table 1. Mesh independence test results

Mesh	Number of elements	Number of nodes	Reynolds number, *Re*	Reduced velocity, U_r	Mean in-line displacement of the isolated cylinder, X_{mean}	Maximum cross-flow displacement of the isolated cylinder, Y_{max}	Strouhal number, *St*
Current study							
Grid 1	40766	20681	100	6	0.0967	0.440	0.164
Grid 2	50037	25332			0.108	0.530	0.1620
Grid 3	61296	30981			0.1217	0.533	0.1620
Grid 4	104061	52421			0.118	0.539	0.1560
Comparison with published literature							
Tu et al. (2015)	-	-	100	6	0.1307	0.525	0.1652
He et al. (2012)	-	-			0.1082	0.503	0.1652
Prasanth and Mittal (2008)	-	-			0.1115	0.529	0.1643

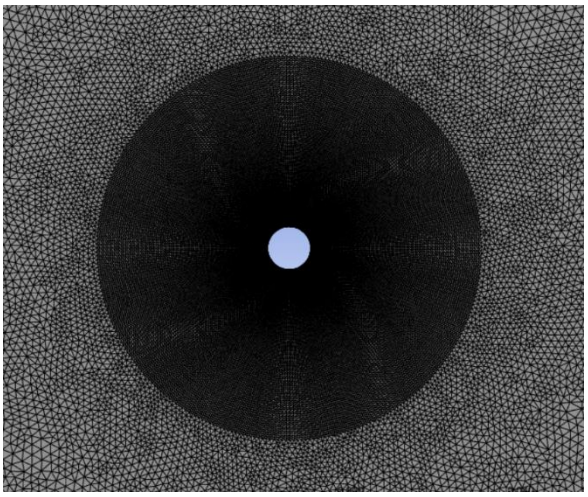

Figure 2. Mesh selected for the simulation.

3. RESULTS AND DISCUSSION

A numerical investigation of two tandem 2DOF cylinders subjected to oscillatory flow at a constant *KC* =10 and different *L/D* ratios is carried out in the present work. This section discusses the vibration amplitudes, transverse vibration frequencies, the spectral content of transverse displacements, and *XY* trajectories of both cylinders at various spacing ratios.

3.1 Lock-in

Figure 3 shows the transverse and streamwise amplitudes of the two tandem cylinders at different spacing ratios as a function of reduced velocity. These amplitudes are compared with the amplitudes of a single isolated cylinder under the same flow conditions. The vibration amplitudes are calculated from the time histories of the

cylinders' displacements over 10 periods of oscillatory flow. The vibration amplitudes are defined as

$A_x = \frac{X_{max} - X_{min}}{2}$ and $A_y = \frac{Y_{max} - Y_{min}}{2}$.

As illustrated in Figure 3, lock-in peaks of both structures and in either direction exhibit two maximums in the given flow conditions during the upper branches. A valley is observed between two peak values in either direction, and this valley is deeper, when a single structure is considered. The transversal vibration has peak amplitudes at U_r = 5 and U_r = 10, whereas the streamwise vibration – at U_r = 9 and U_r = 11. In Figure 3, both the single cylinder and the two tandem cylinders exhibit maximum transverse amplitude at a reduced velocity of 10, with the single cylinder reaching the highest transverse amplitude of 1.25*D*. According to Jauvtis and Williamson (2004), the transverse amplitude in the "super-upper" branch can reach as high as 1.5*D*. Another important feature of the 2DOF structure vibration in the oscillatory flow is that the streamwise peak is overall about twice higher than the transversal peak, which is directly in contrast with lock-ins experienced in uniform flows.

The work by Zhao et al. (2013) reports that the transverse amplitude is comparable to the streamwise amplitude as the reduced velocity is below a critical value. Once the reduced velocity exceeds this value, the transverse amplitude becomes smaller than the streamwise amplitude, and the difference between the two increases with increasing reduced velocity. At a reduced velocity of 2 in the current study, both amplitudes are comparable. For $3 \leq U_r \leq 5$, the transverse amplitude exceeds the in-line amplitude. However, beyond a reduced velocity of 5, the in-line amplitude becomes significantly larger than the cross-flow amplitude. At $U_r \geq 11$, the cross-flow amplitude nearly vanishes, so that the lower branch of the streamwise lock-in peak is significantly higher than for the transversal direction.

It is evident from Figure 3 that in oscillatory flow, spacing ratio has no significant influence on the vibration response of the cylinders. The tandem cylinder responses show similar patterns to those of the single cylinder. However, at a spacing ratio of *L/D* = 4.5, the Cylinder 2 shows a slight deviation in the trend of the cross-flow amplitude. Also, at $5 \leq U_r \leq 8$, the streamwise vibration amplitudes appear to be lower in the case of a single structure.

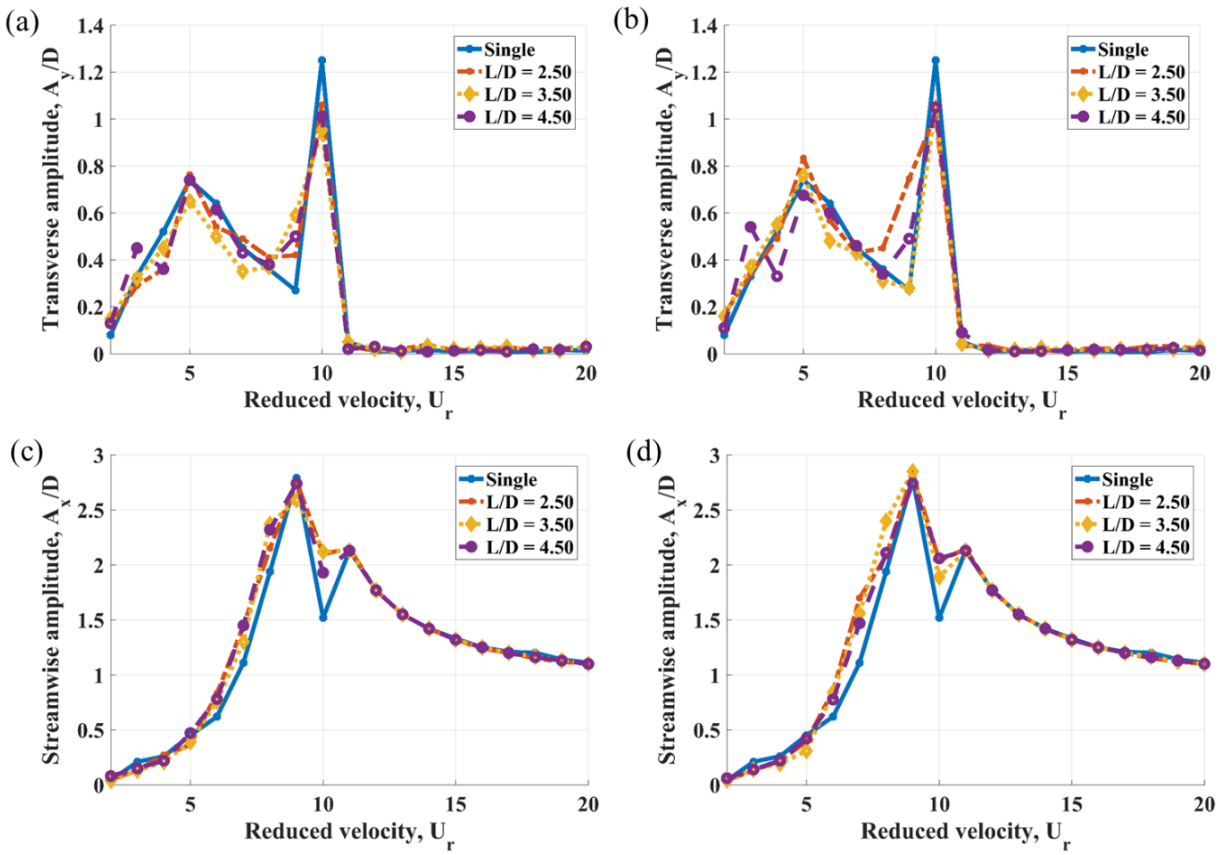

Figure 3. Displacement amplitudes at different *L/D* ratios: (a) in transversal direction for Cylinder 1; (b) in transversal direction for Cylinder 2; (c) in streamwise direction for Cylinder 1; and (d) in streamwise direction for Cylinder 2

3.2 Transverse frequency ratio

Figure 4 presents the transverse frequency ratio $\frac{f_{yp}}{f_w}$ for Cylinders 1 and 2 as a function of reduced velocity, where f_{yp} is the dominating transverse vibration frequency, and f_w is the oscillatory flow frequency (Zhao et al., 2011, January). A Fast Fourier Transform (FFT) is applied to analyze the displacement frequencies. While the streamwise vibration frequency matches the frequency of the oscillatory flow, the transverse vibration frequency exhibits a different behavior. The oscillatory flow frequency is in the range of 0.154-1.541 Hz at reduced velocity of 2-20 respectively.

According to Zhao et al. (2013) and Zhao et al. (2011, January), the transverse vibration frequency decreases with increasing reduced velocity at a constant *KC* number which agrees well with the present results. The analysis also shows that the spacing ratio has no significant effect on the frequency behavior of the two tandem cylinders. For reduced velocities in the range $4 \leq U_r < 10$, the transverse vibration frequency is approximately twice that of the oscillatory flow, which aligns with experimental findings of Kozakiewicz et al. (1997) and Sumer and Fredsøe (1988). At a reduced velocity of 10, a lock-in is observed, as the frequency of the structure, transverse displacement and oscillatory flow coincide, and the maximum vibration amplitude occurs.

Previous studies by Zhao et al. (2011, January), Sumer and Fredsøe (1988) and Zhao et al. (2012) reveal that a circular cylinder in purely oscillatory flow can vibrate transversally at frequencies that are integer multiples of the flow frequency. The work by Zhao et al. (2012) identifies the following vibration modes, based on the oscillation frequency. If a cylinder oscillates mainly with a frequency equal to the frequency of the oscillatory flow, the oscillation is in a single-frequency mode. A double-frequency mode means that the vibration frequency is twice as the oscillatory flow frequency, etc. In this present work, the vibration mode of the cylinder changes from a double-frequency mode at $4 \leq U_r < 10$ and then to a single-frequency mode at a reduced velocity of 10.

Figures 5 and 6 show the amplitude spectra of the cross-flow displacement of the tandem cylinders at a spacing ratio of *L/D* = 2.5 at a range of reduced velocities. Oscillations during the initial branch are mostly governed by a single dominant frequency, as in Figure 5, while multiple peaks are present in the signals corresponding to the lower branch on lock-in in Figure 6. Majority of the dominant frequencies fall into the range from 0.5 to 0.77 Hz, which is close to the natural frequency of the structure, while the oscillatory flow frequency varies.

3.3. Lift coefficient

Figure 7 illustrates the root mean square (RMS) lift coefficient $C_{L,rms}$ of Cylinders 1 and 2 as a function of reduced velocity at various spacing ratios. As U_r increases from 2 to 8, $C_{L,rms}$ grows approximately exponentially, reflecting strengthening of vortex shedding during the initial and upper branches of the lock-in. The peak at U_r = 8 coincides with the onset of strong transverse oscillations (Figure 3). The influence of spacing ratio on the RMS lift coefficient is visible in the $C_{L,rms}$ peak height for Cylinder 1 in Figure 7(a). The maximum RMS value of the lift coefficient for both cylinders occurs at a reduced velocity of 8 for L/D = 2.50. Beyond U_r = 10, $C_{L,rms}$ gradually decays, mirroring the collapse of cross-flow amplitudes.

3.4. *XY* trajectories

Figures 8, 9 and 10 show the *XY* trajectories of the cylinders' displacement at a spacing ratio of *L/D* = 2.5 for selected reduced velocities. The trajectories of the tandem cylinders appear to be similar at each spacing ratios and distinct mode of vibration are observed at certain reduced velocities. For reduced velocities of $6 \leq U_r \leq 9$, infinity-like (∞) mode is observed at each spacing ratio. This agrees with the work of Zhao et al. (2011, January). The slight tilt of the infinity loops might indicate a nonzero phase shift between the two motion components, characteristic of a double-frequency mode (Zhao et al. 2011, January, Zhao et al., 2012).

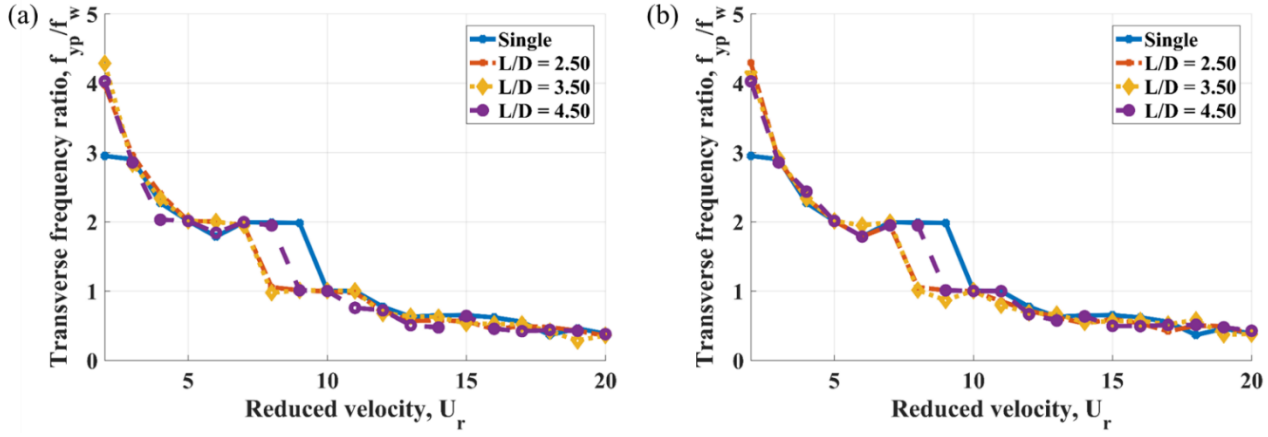

Figure 4. Transverse frequency ratio at different *L/D* ratios: (a) for Cylinder 1 and (b) for Cylinder 2

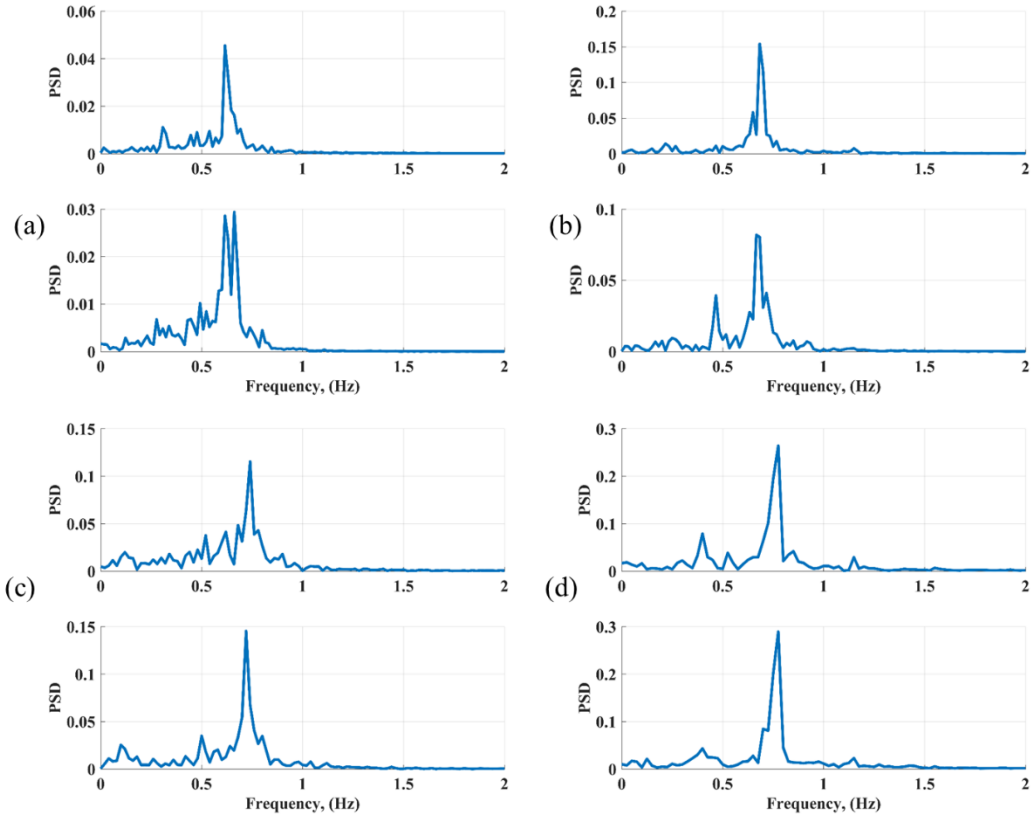

Figure 5. Power spectrum density (PSD) at L/D = 2.5 for: (a) U_r = 2; (b) U_r = 3; (c) U_r = 4; and (d) U_r = 5. Top diagrams are for Cylinder 1, and bottom diagrams are for Cylinder 2

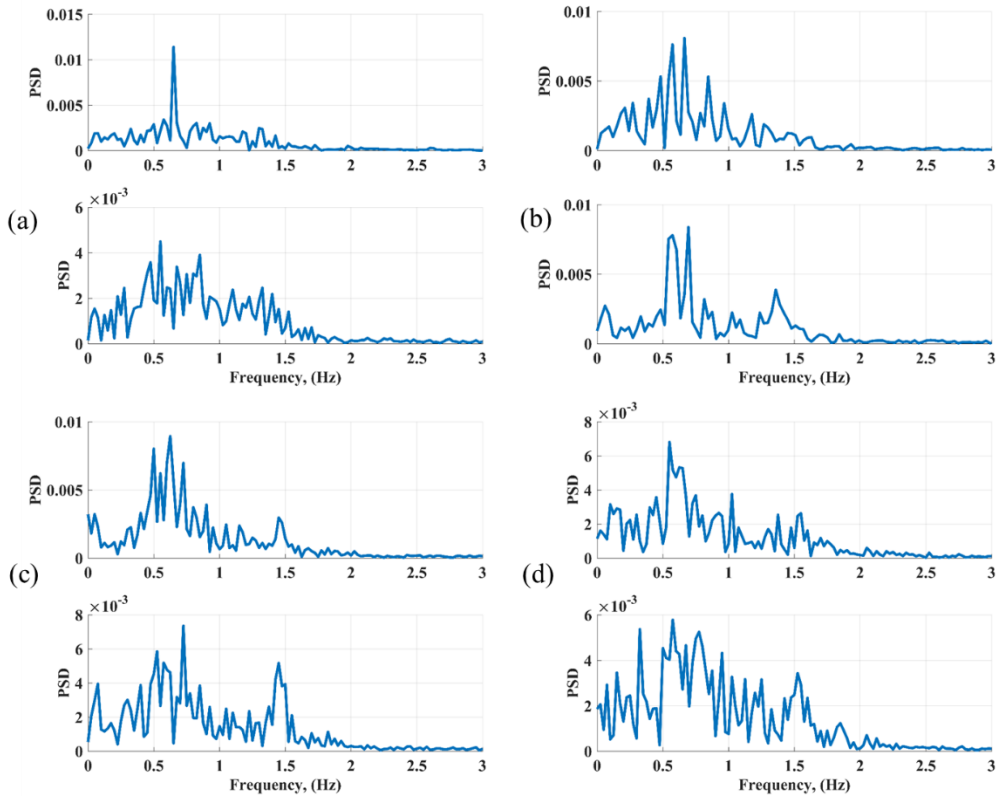

Figure 6. Power spectrum density diagrams at L/D = 2.5 for: (a) U_r = 17; (b) U_r = 18; (c) U_r = 19; and (d) U_r = 20. Top diagrams are for Cylinder 1, and bottom diagrams are for Cylinder 2

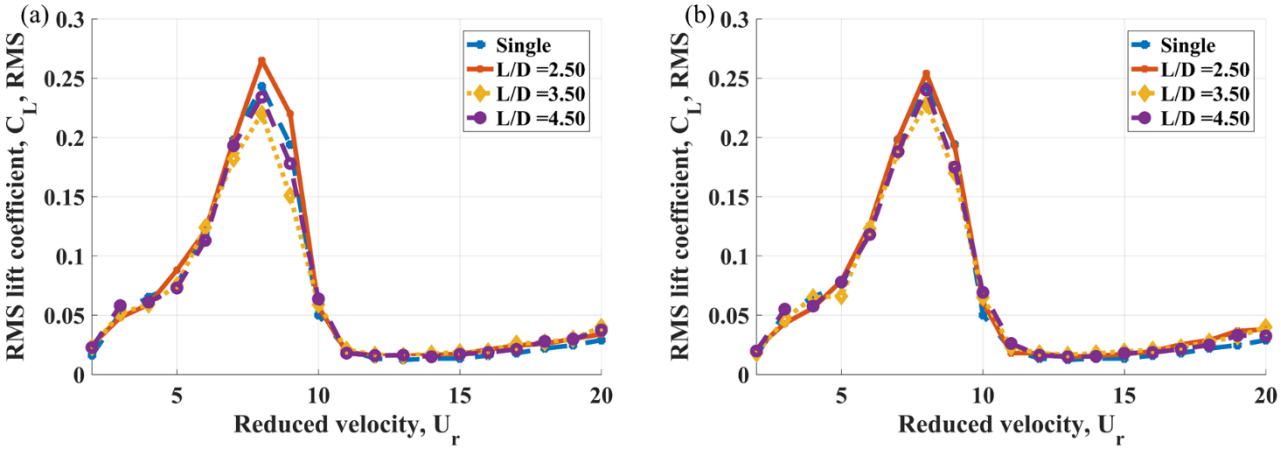

Figure 7. RMS lift coefficient for: (a) Cylinder 1; and (b) Cylinder 2

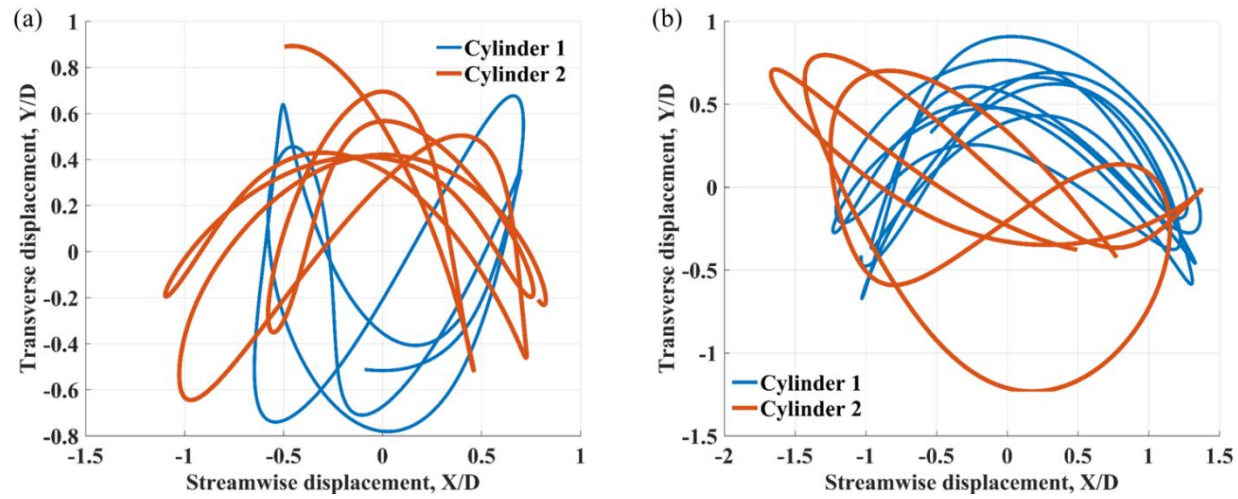

Figure 8. *XY* trajectories at *L/D* = 2.5 for: (a) U_r = 6; and (b) U_r = 7

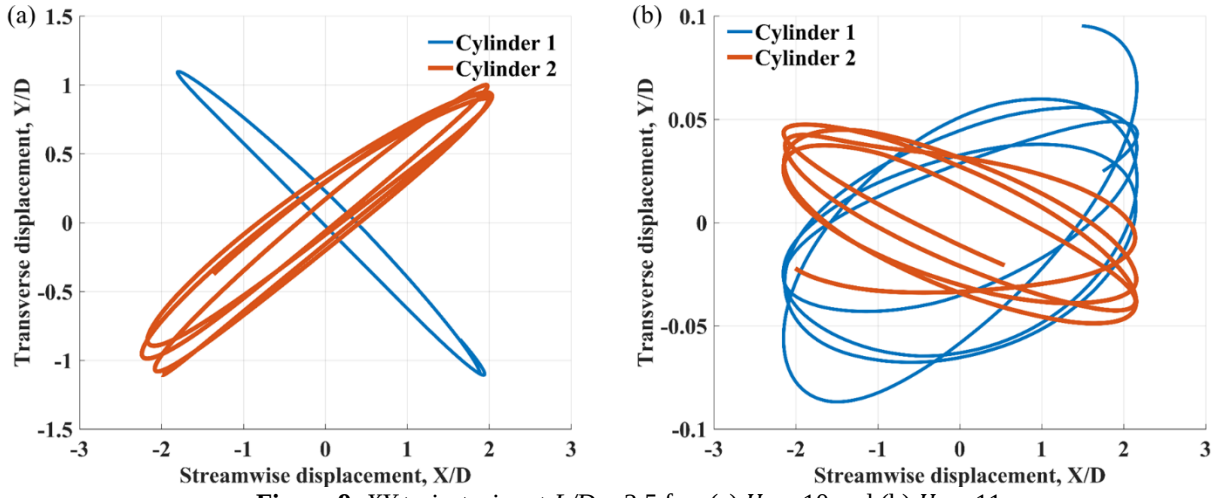

Figure 9. *XY* trajectories at *L/D* = 2.5 for: (a) U_r = 10 and (b) U_r = 11

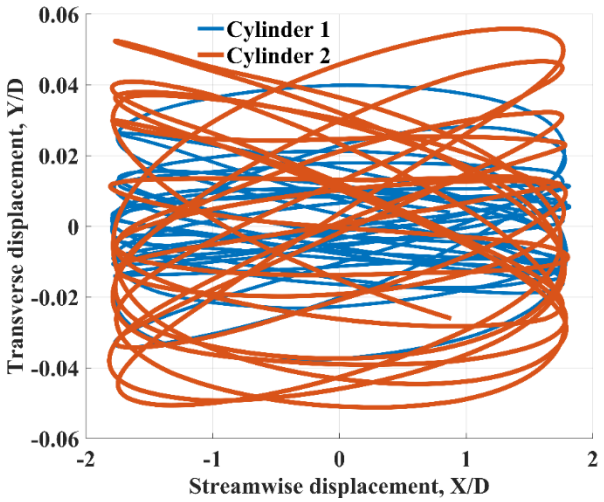

Figure 10. *XY* trajectory at *L/D* = 2.5 for U_r = 12

At a reduced velocity of 10, an arc-like mode is identified. The motion is dominated by large transverse peaks with relatively smaller in-line offsets. The path resembles a bow or C-shape. At a reduced velocity of 11, the mode of the displacement appears to be in an O-shape, and for $U_r \geq 12$, the motion of cylinders is mainly in-line with a net-like shape, as shown in Figure 10. The cross-flow amplitude is reduced to near zero. This post-lock-out regime demonstrates that the cylinder no longer engages strongly with vortex shedding; its motion is driven passively by the inlet velocity oscillation alone.

4. CONCLUSIONS

This study investigates the vortex-induced vibration of two tandem circular cylinders with two degrees of freedom under pure oscillatory flow conditions. The computational domain is designed to accommodate various spacing ratios between the cylinders, ranging from 2.5 to 4.5. The primary focus of the investigation is to analyze the transverse and streamwise vibration amplitudes, frequency ratios, spectral frequencies, and *XY* displacement trajectories of both cylinders, as well as to compare them with a single isolated cylinder under the same flow conditions. The study successfully validates the computational model through mesh independence tests. The validation demonstrates good agreement, confirming the accuracy and reliability of the simulation setup.

Key Findings include the following.

1. Amplitude and Vibration Characteristics:
   - Streamwise displacement amplitude exceeds 2.5D for both cylinders and for a single structure.
   - The maximum transverse amplitude for both tandem cylinders is observed at a reduced velocity of 10.
   - The single isolated cylinder exhibits a higher maximum transverse amplitude (1.25D) compared to the tandem configuration.
   - No significant influence of the spacing ratio on the maximum vibration amplitude is observed.
2. Frequency Ratio and Spectral Analysis:
   - The transverse vibration frequencies of the tandem cylinders display mode transition behavior with the increasing reduced velocity. A double-frequency mode is identified at reduced velocity of $4 \leq U_r < 10$, followed by a single-frequency mode at U_r = 10.
   - The spacing ratio has negligible effects on the transverse frequency ratio, confirming that tandem configurations do not significantly alter the primary vibration frequencies.
3. Trajectory and Mode Transition:
   - The *XY* trajectory analysis shows distinct vibration modes at various reduced velocities.
   - An infinity (∞) shape is observed in the range of $6 \leq U_r \leq 9$.
   - An arc-like mode appears at U_r = 10.
   - At U_r = 11, the motion transforms into an O-shape, while for $U_r \geq 12$, the vibration mode becomes predominantly in-line with a net-like pattern.

The findings of this study provide valuable insights into the dynamic behavior of tandem circular cylinders subjected to oscillatory flows. The transition between different vibration modes, especially the occurrence of lock-in at a reduced velocity of 10, highlights the critical regions where structural responses could become significantly amplified, posing potential risks to engineering structures such as offshore platforms and pipeline systems.

Acknowledgements: The authors would like to acknowledge the support of the Ministry of Science and Higher Education of the Russian Federation, grant number FEWN-2024-0005. V.K. would like to thank Dr. A. Postnikov for the productive discussions on CFD simulations on VIV of 2DOF rigid structures.

References:

An, H. (2009). Numerical modelling of flow characteristics and hydrodynamic forces on a cylinder subject to oscillatory flow.

An, H., Cheng, L., & Zhao, M. (2009). Steady streaming around a circular cylinder in an oscillatory flow. *Ocean Engineering*, *36*(14), 1089-1097. https://doi.org/10.1016/j.oceaneng.2009.06.010

An, H., Cheng, L., & Zhao, M. (2011). Direct numerical simulation of oscillatory flow around a circular cylinder at low Keulegan–Carpenter number. *Journal of Fluid Mechanics*, *666*, 77-103. https://doi.org/10.1017/S0022112010003691

An, H. W., Cheng, L., Zhao, M., & Dong, G. H. (2006). Numerical simulation of the oscillatory flow around two cylinders in tandem. *Journal of Hydrodynamics*, *18*, 189-195. https://doi.org/10.1007/BF03400445

An, H., Cheng, L., Zhao, M., & Dong, G. (2006, January). Numerical simulation of oscillatory flow around two circular cylinders of different diameters. In *International Conference on Offshore Mechanics and Arctic Engineering* (Vol. 47470, pp. 35-43). https://doi.org/10.1115/OMAE2006-92033

Annapeh, H. F., & Kurushina, V. (2024). Transversal Vortex-Induced Vibration of a Circular Cylinder in Tandem with a Stationary Square Structure. *Applied Mechanics*, *5*(4), 978-996. https://doi.org/10.3390/applmech5040054

Barbi, C., Favier, D. P., Maresca, C. A., & Telionis, D. P. (1986). Vortex shedding and lock-on of a circular cylinder in oscillatory flow. *Journal of Fluid Mechanics*, *170*, 527-544. https://doi.org/10.1017/S0022112086001003

Bearman, P. W. (1984). Vortex shedding from oscillating bluff bodies. *Annual review of fluid mechanics*, *16*, 195-222. https://doi.org/10.1146/annurev.fl.16.010184.001211

Bearman, P. W., Downie, M. J., Graham, J. M. R., Obasaju, E.D. (1985). Forces on cylinders in viscous oscillatory flow at low Keulegan–Carpenter numbers. *Journal of Fluid Mechanics*, *154*, 337–356. https://doi.org/10.1017/S0022112085001562

Bushnell, M. J. (1977, May). Forces on cylinder arrays in oscillating flow. In *Offshore Technology Conference* (pp. OTC-2903). OTC. https://doi.org/10.4043/2903-MS

Chern, M. J., Kanna, P. R., Lu, Y. J., Cheng, I. C., & Chang, S. C. (2010). A CFD study of the interaction of oscillatory flows with a pair of side-by-side cylinders. *Journal of Fluids and Structures*, *26*(4), 626-643. https://doi.org/10.1016/j.jfluidstructs.2010.03.002

He, T., Zhou, D., & Bao, Y. (2012). Combined interface boundary condition method for fluid–rigid body interaction. *Computer Methods in Applied Mechanics and Engineering*, *223*, 81-102. https://doi.org/10.1016/j.cma.2012.02.007

Jauvtis, N. A., & Williamson, C. H. K. (2004). The effect of two degrees of freedom on vortex-induced vibration at low mass and damping. *Journal of Fluid Mechanics*, *509*, 23-62. https://doi.org/10.1017/S0022112004008778

Justesen, P. (1991). A numerical study of oscillating flow around a circular cylinder. *Journal of Fluid Mechanics*, *222*, 157-196. DOI: https://doi.org/10.1017/S0022112091001040

Keulegan, G. H., & Carpenter, L. H. (1958). Forces on cylinders and plates in an oscillating fluid. *Journal of Research of the National Bureau of Standards*, *60*(5), 423-440.

Kozakiewicz, A., Sumer, B. M., Fredsøe, J., & Hansen, E. A. (1997). Vortex regimes around a freely vibrating cylinder in oscillatory flow. *International Journal of Offshore and Polar Engineering*, *7*(02).

Lu, L., Zhou, Z., & Zhang, C. (2023). Flow regime identification and flow instability analysis of oscillatory flows over twin circular cylinders. *Physics of Fluids*, *35*(10). https://doi.org/10.1063/5.0160260

Meneghini, J. R., & Bearman, P. W. (1995). Numerical simulation of high amplitude oscillatory flow about a circular cylinder. *Journal of fluids and structures*, *9*(4), 435-455. https://doi.org/10.1006/jfls.1995.1025

Obasaju, E. D., Bearman, P. W., & Graham, J. M. R. (1988). A study of forces, circulation and vortex patterns around a circular cylinder in oscillating flow. *Journal of Fluid Mechanics*, *196*, 467-494. https://doi.org/10.1017/S0022112088002782

Pearcey, T., Zhao, M., Xiang, Y., & Liu, M. (2017). Vibration of two elastically mounted cylinders of different diameters in oscillatory flow. *Applied Ocean Research*, *69*, 173-190. https://doi.org/10.1016/j.apor.2017.11.003

Prasanth, T. K., & Mittal, S. (2008). Vortex-induced vibrations of a circular cylinder at low Reynolds numbers. Journal of Fluid Mechanics, 594, 463-491. https://doi.org/10.1017/S0022112007009202

Ren, C., Cheng, L., Tong, F., Xiong, C., & Chen, T. (2019). Oscillatory flow regimes around four cylinders in a diamond arrangement. *Journal of Fluid Mechanics*, *877*, 955-1006. https://doi.org/10.1017/jfm.2019.609

Ren, H., Zhang, M., Wang, Y., Xu, Y., Fu, S., Fu, X., & Zhao, B. (2020). Drag and added mass coefficients of a flexible pipe undergoing vortex-induced vibration in an oscillatory flow. *Ocean Engineering*, *210*, 107541. https://doi.org/10.1016/j.oceaneng.2020.107541

Sarpkaya, T. (1986). Force on a circular cylinder in viscous oscillatory flow at low Keulegan—Carpenter numbers. *Journal of Fluid Mechanics*, *165*, 61-71. https://doi.org/10.1017/S0022112086002999

Sarpkaya, T., & Storm, M. (1985). In-line force on a cylinder translating in oscillatory flow. *Applied Ocean Research*, *7*(4), 188-196. https://doi.org/10.1016/0141-1187(85)90025-2

Skomedal, N. G., Vada, T., & Sortland, B. (1989). Viscous forces on one and two circular cylinders in planar oscillatory flow. *Applied ocean research*, *11*(3), 114-134. https://doi.org/10.1016/0141-1187(89)90022-9

Sumer, B. M., & Fredsøe, J. (1988). Transverse vibrations of an elastically mounted cylinder exposed to an oscillating flow. *Journal of Offshore Mechanics and Arctic Engineering*, *110(4)*, 387-394. DOI: https://doi.org/10.1115/1.3257077

Sumer, B.M., & Fredsøe, J. (1997). Hydrodynamics around Cylindrical Structures. World Scientific, Singapore, River Edge, NJ.

Tatsuno, M., & Bearman, P. W. (1990). A visual study of the flow around an oscillating circular cylinder at low Keulegan–Carpenter numbers and low Stokes numbers. *Journal of Fluid Mechanics*, *211*, 157-182. https://doi.org/10.1017/S0022112090001537

Tong, F., Cheng, L., Zhao, M., & An, H. (2015). Oscillatory flow regimes around four cylinders in a square arrangement under small KC and Re conditions. *Journal of Fluid Mechanics*, *769*, 298-336. https://doi.org/10.1017/jfm.2015.107

Tu, J., Zhou, D., Bao, Y., Ma, J., Lu, J., & Han, Z. (2015). Flow-induced vibrations of two circular cylinders in tandem with shear flow at low Reynolds number. *Journal of Fluids and Structures*, *59*, 224-251. https://doi.org/10.1016/j.jfluidstructs.2015.08.012

Williamson, C. H. K. (1985). Sinusoidal flow relative to circular cylinders. *Journal of Fluid Mechanics*, *155*, 141-174. https://doi.org/10.1017/S0022112085001756

Zhang, M., Fu, S., Ren, H., Xu, Y., & Qin, X. (2022). Experimental investigation on vortex-induced force of a flexible pipe under oscillatory flow. *Applied Ocean Research*, *126*, 103269. https://doi.org/10.1016/j.apor.2022.103269

Zhao, M. (2013). Numerical investigation of two-degree-of-freedom vortex-induced vibration of a circular cylinder in oscillatory flow. *Journal of Fluids and Structures*, *39*, 41-59. https://doi.org/10.1016/j.jfluidstructs.2013.02.003

Zhao, M., & Cheng, L. (2014). Two-dimensional numerical study of vortex shedding regimes of oscillatory flow past two circular cylinders in side-by-side and tandem arrangements at low Reynolds numbers. *Journal of fluid mechanics*, *751*, 1-37. https://doi.org/10.1017/jfm.2014.268

Zhao, M., Cheng, L., & An, H. (2012). Numerical investigation of vortex-induced vibration of a circular cylinder in transverse direction in oscillatory flow. *Ocean Engineering*, *41*, 39-52. https://doi.org/10.1016/j.oceaneng.2011.12.017

Zhao, M., Cheng, L., & Zhou, T. (2011, January). Numerical investigation of vortex-induced vibration (VIV) of a circular cylinder in oscillatory flow. In *International Conference on Offshore Mechanics and Arctic Engineering* (Vol. 44397, pp. 597-603). DOI: https://doi.org/10.1115/OMAE2011-50074

Zhao, M., Kaja, K., Xiang, Y., & Yan, G. (2013). Vortex-induced vibration (VIV) of a circular cylinder in combined steady and oscillatory flow. *Ocean Engineering*, *73*, 83-95. https://doi.org/10.1016/j.oceaneng.2013.08.006

Henry Francis Annapeh
Industrial University of Tyumen,
Tyumen,
Russia
kinghenry939@gmail.com
ORCID 0000-0003-1256-499X

Victoria Kurushina
Industrial University of Tyumen,
Tyumen,
Russia
v.kurushina@outlook.com
ORCID 0000-0001-9294-5789